A Study of High Specific Impulse Ion Thruster Optics

Paul J. Wilbur, Joshua Miller, Cody Farnell
Department of Mechanical Engineering
Colorado State University
Fort Collins, CO 80523
970-491-8564
pwilbur@engr.colostate.edu
and
Vincent K. Rawlin
NASA Glenn Research Center
Cleveland, OH 44135
216-977-7462
vince.rawlin@grc.nasa.gov

IEPC-01-098

An experimental study conducted on nineteen-hole-pair, two-grid optics sets suitable for operation at high specific impulse is described. Perveance and crossover beamlet current limits above and below which accelerator grid direct impingement currents rise are measured. Accelerator grid voltages required to prevent electron backstreaming are shown to be modest. The importance of selecting screen grid thickness to prevent accelerator grid sputtering by ions drawn from upstream of screen grid webs is illustrated. Experimental results are compared to numerical results obtaining using the "igx"code and shown to be in reasonable agreement. Results from the code suggest that grid systems of reasonable size and with long lives can be designed for high specific impulse missions.

Nomenclature

d – grid hole diameter (mm)
D – beam diameter (cm)
e – electron charge (coul)
F – flatness parameter
J – current (mA)
ℓ – separation distance (mm)
m – krypton ion mass (kg)
$\dot{m}$ – krypton flow rate (mA eq)
t – grid thickness (mm)
V – voltage (V or kV)
w – min. grid webbing thickness (mm)
ε_o – permittivity of free space (f/m)
η_u – propellant utilization efficiency
$\wp$ - normalized perveance per hole

subscripts
a – accelerator grid
b – beamlet (i.e. per hole)
B – beam
g – between screen and accelerator grids
i – impingement per beamlet
N – net
s – screen grid
sh – between screen grid and sheath
T - total

Introduction

For many years, electric propulsion mission emphases have been on near-earth applications, characterized by relatively low specific impulses and modest power levels. Ion thruster development has, as a consequence, been focused on maximization of thrust density within a framework of general improvement in thruster reliability and lifetime. Renewed interest in the exploration of interstellar space under the NASA Origins Program is accompanied by the need for high specific impulse, high power propulsion. Ion propulsion systems are well suited to this application because the modifications needed to change them so they can be operated at high specific impulse and high power rather than low specific impulse and a more modest power are quite straightforward. This paper addresses the part of ion thruster design that is changed substantially, namely, the design of the ion extraction optics (grids).

Although the main emphasis of this work has been experimental, it has been guided by numerical analysis. Further, a simple analytical model is used to estimate the impact of results obtained from the study on a typical mission. The goal of the work has been to generate a body of data from which grid system geometrical and operating parameters could be defined to accomplish a specified mission objective. The study will be focused around ion extraction grid design for a nominal 30-kW ion propulsion module operating on krypton at a specific impulse of 14,000 s for 88,000 h (10 years) [1]. Assuming operation at a thruster propellant utilization efficiency near 80%, these power and specific impulse values correspond to a net accelerating voltage of 13 kV and an ion beam current of 2.3 A.

Apparatus and Procedures

Experimental studies were conducted using two-grid, nineteen-aperture-pair assemblies that were configured as shown in Fig. 1 and mounted to a ring-cusp discharge chamber [2]. Most of the data reported here were collected with twelve different grid geometrical configurations. The grids were made of stainless steel and were separated and isolated from each other using three, 12.7-mm diam. synthetic sapphire balls that were clamped between sputter-shielded assemblies attached to the grids. These spheres would frequently glow but they did not conduct measurable current when voltage differences as great as 15 kV were applied between them.

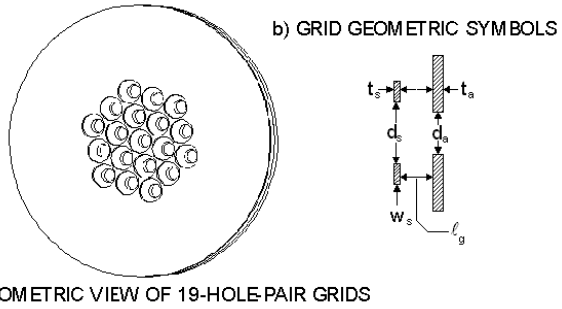

Fig. 1 Grid System

The discharge chamber anode diameter was 15 cm and the largest diameter of the screen grid region over which ions were extracted on the discharge chamber centerline was 4.7 cm. Because the ion extraction region is a small fraction of the plasma diameter, it is argued that all nineteen of the screen grid holes will see the same discharge plasma conditions. Hence, it is argued that the ion extraction behavior should be about the same for each screen/accelerator hole pair, and that measured beam and impingement currents can be divided by nineteen to obtain per hole (beamlet) values. Additional verification that this is the case was obtained by using a Faraday probe [3] swept through the beam 2 cm downstream of the accelerator grid to measure beam current density profiles. Figure 2 shows a typical

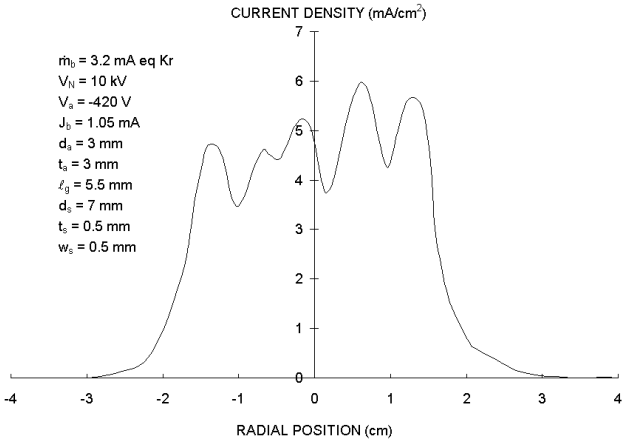

Fig. 2 Typical Current Density Profile for a nineteen-hole Grid Set

profile measured when the probe was swept on an arc through the thruster centerline. It shows a peak for each of the five beamlets that differ by only about 10%. It is believed that the peak current densities would be more nearly equal if the probe could have been swept along the line on which the holes are located rather than on an arc that passed over the centerlines of some holes and the edges of others. It is noted that the current sensor diameter is 5.2 mm and that numerical results suggest that the bulk of the beam current from each hole is concentrated in a much smaller diameter. Hence, it does not sense the structure of the beamlets precisely and the beam current determined by integrating Fig. 2 is, as a result, greater than the measured current.

Ion beam neutralization was generally accomplished using two tungsten wires that passed through the beam. A 3.2-mm diam., krypton hollow cathode neutralizer equipped with a 0.2-mm diam. orifice was used in some tests and it was demonstrated that results obtained using the filament and hollow cathodes were the same.

Tests were conducted in a 45-cm diam. vacuum bell jar test facility. Pre-test pressures in the chamber were about $3x10^{-6}$ Torr, but they varied through the range from $5x10^{-5}$ to $1.8x10^{-4}$ Torr as total flow rate was varied from 60 to 150 mA eq. Kr.

After the establishment of stable flow and operating conditions, the tests generally involved measurement of beam current and accelerator grid impingement current as discharge power, screen grid voltage or accelerator grid voltage were varied. On some occasions, however, the beamlet cross section was measured by sputter eroding through a 0.013–mm thick Ta foil spot-welded to the upstream side of the accelerator grid. Although tests were conducted at net accelerating voltages of 10 and 13 kV using grids with screen hole diameters of 7-mm and 9-mm emphasis will be given, to data obtained using the screen grid with 9-mm holes operating at 13-kV in this paper.

Results

Screen Grid Sheath Effects

The initial design of the 19-hole screen grid to be used in these tests was thin (0.5 mm) compared to the screen grid hole diameter (7 mm). A thin grid was used because it was argued it would produce a sheath that would be substantially upstream of the screen grid. In this location it was believed the sheath would be able to extract most of the ions incident upon it through the screen grid thereby reducing screen grid erosion and improving discharge chamber performance. Initial tests made the drawbacks of such a design obvious.

Figure 3 shows typical erosion patterns produced on Ta foils covering 3-mm diameter accelerator grid holes after about an hour of operation. For about a minute, the foil at an erosion site would be white-hot and the impingement current would be high and then the foil would cool as the impingement current dropped to near normal for the rest of the test.

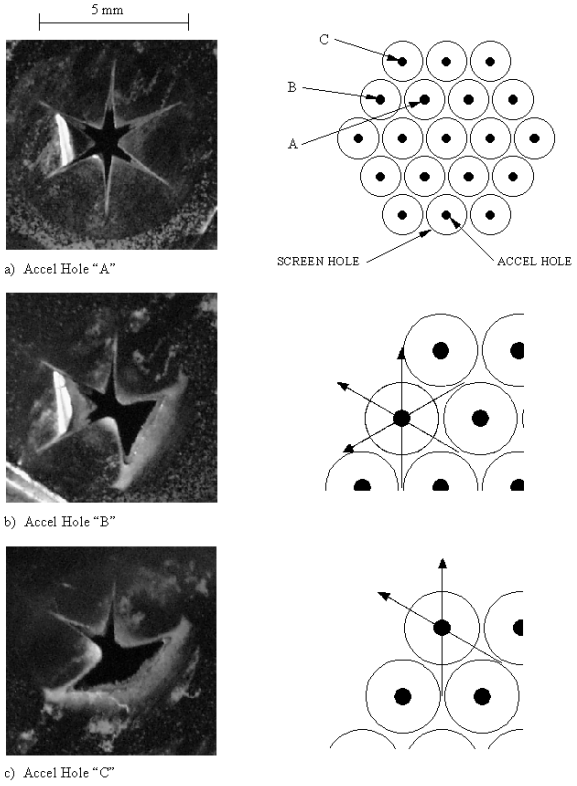

Fig. 3 Beamlet Current Patterns at Accelerator Grid

The sketch in the upper right hand corner of Fig. 3 shows the grid-hole sets, as they would be viewed from the discharge chamber. Figure 3a shows the star pattern

eroded in the foil over the "A" hole identified in the sketch. Six holes and six webs surround this hole and the star has six points. The erosion pattern for hole "B" from the sketch, which is shown in Fig. 3b, is surrounded by four holes and three webs and has three sharp points. Similarly, hole "C", which is surrounded by three holes and two webs, has two sharp points. On the basis of these observations it is concluded that the points are associated with the webs. The alignment of the points relative to the webs suggests that the erosion of the points is being produced by ions drawn from the region upstream of the screen-grid web and accelerated diagonally across the hole-pair axis and into the upstream side of the accelerator grid. The path of ions that erode the peaks is suggested by the arrows in the sketches to the right of Figs. 3b and 3c. It is noted that the bright spots on the left sides of Figs. 3a and 3b are caused by reflections from small wrinkles in the foils.

The effect of beamlet current and screen grid thickness on the pattern of an accelerator hole surrounded by six other holes is illustrated in Fig. 4. All of the operating and geometrical parameters except the beamlet current were the same for the two patterns shown in Fig. 3a and 3b but the 1.05 mA pattern was run for a shorter time to hold the total ion dose about the same. Comparison of the photographs suggests a greater concentration of current near the hole center and shorter points for the greater beamlet current. This is consistent with the fact that the sheath to screen grid separation would be less at the higher beam current. Comparison of Figs. 4a and 4c shows the dramatic effect of an increase in screen grid thickness on the erosion pattern obtained with an otherwise identical geometry at a beamlet current of 0.58 mA. With the thicker screen grid, it is argued that the edge of the sheath does not extend substantially upstream of the upstream edge of a screen grid hole. As a result interaction between the sheaths at adjacent holes is minimized, ions are not drawn from upstream of the screen grid webs and the sharp points in the foil are not produced.

Backstreaming Limitations

The magnitude of the negative voltage that must be applied to the accelerator grid to prevent electron backstreaming was measured at each beamlet current and grid geometry condition investigated. The

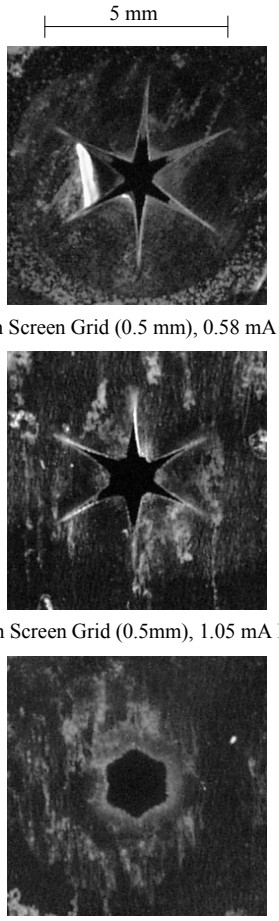

a) Thin Screen Grid (0.5 mm), 0.58 mA Beamlet

b) Thin Screen Grid (0.5mm), 1.05 mA Beamlet

c) Thick Screen Grid (1.5 mm), 0.58 mA Beamlet

Fig. 4 Effect of Screen Grid Thickness and Current on Beamlet Pattern

magnitude of this voltage could be a major design driver for high specific impulse grids if it increased along with net accelerating voltage. If this did occur, then charge-exchange ion sputtering damage could be expected to increase and this would shorten accelerator grid lifetimes.

A typical curve showing the sudden increase in apparent beamlet current that occurs when the magnitude of this voltage is insufficient to prevent backstreaming is given in Fig. 5. The ordinate in this plot is the ratio of beamlet currents at $|V_a|$ and at a voltage significantly greater than the backstreaming limit, namely $|V_a| = 500$ V. At the backstreaming limit electrons drawn upstream from the beam into the discharge chamber cause the increase in apparent

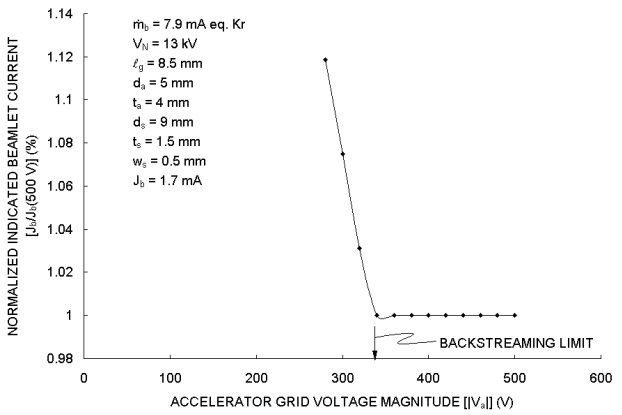

Fig. 5 Effect of Accelerator Grid Voltage on Electron Backstreaming

beamlet current.

Backstreaming limits like the one identified shown in Fig. 5 were determined as a function of beamlet current and grid geometrical changes. The results obtained in this way are plotted in Fig. 6 for various grid spacings and for an accelerator hole diameter of 4.5 mm.

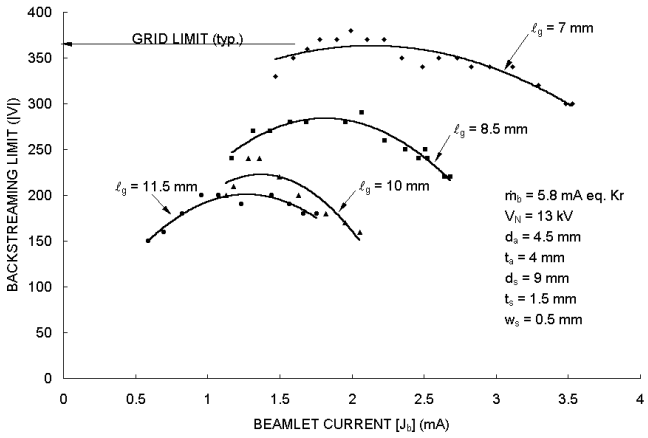

Fig. 6 Effects of Grid Separation and Beamlet Current on Backstreaming

There is obvious scatter in these data, but all appear to follow the same general trend in which the peak backstreaming limit is observed at a current intermediate between typical maximum and minimum values associated with each grid spacing. The intermediate current at which these curves peak corresponds to the beamlet focusing condition where positive space charge is most conducive to electron backstreaming.

A full-sized thruster operating at beamlet currents over the full range between the maximum and minimum values associated with each of the curves in Fig. 6 would have to operate with the accelerator grid biased to the maximum limit (identified as the grid limit for the upper curve). Adding a 30-V margin against backstreaming to these maxima and plotting the results as a function of accelerator hole diameter with grid separation as a parameter, one obtains the results shown by the solid symbols and finer lines in Fig. 7. The data identified by the open symbols and heavier lines are values predicted by the "igx" code applying the same margin [4].

Both sets of data exhibit similar trends although the numerical results are 50 to 100 V greater than the measured values. All of the data generally show that the accelerator grid voltage magnitude required to prevent backstreaming increases as the grid separation is reduced or the accelerator hole diameter is increased. These trends are consistent with theory and data obtained on low specific impulse thrusters.

It is important to note that the voltages required to limit backstreaming through accelerator grids that are given in Fig. 7 for high specific impulse grids do not differ much from those required for low specific impulse grids. This reflects the fact that the backstreaming limit depends mostly on the intragrid electric field rather than the net accelerating voltage.

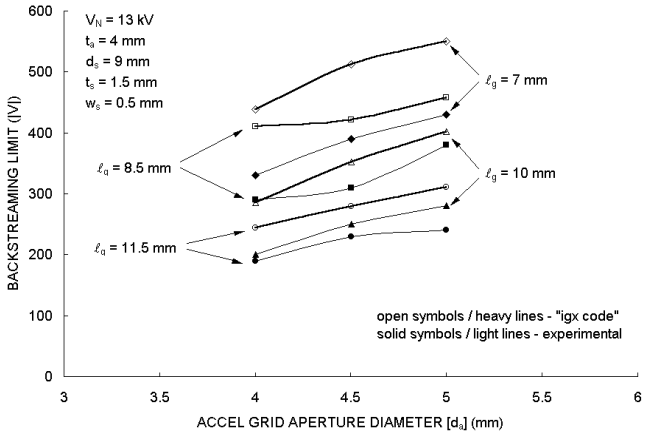

Fig. 7 Effects of Accelerator Grid Hole Diameter and Grid Separation on Backstreaming

Direct Ion Impingement Limitations

A common way to assure that direct erosion of the accelerator grid by beam ions is not occurring in a grid set is to hold beam current constant and measure impingement current as a function of net accelerating voltage [5]. This usually yields a limit on screen grid voltage, below which the impingement current rises. When this was done in the course of the present study, data like those shown in Fig. 8 were obtained. Under high net accelerating voltage test conditions this figure shows that both a perveance (lower) limit and a crossover (higher) limit were observed. The higher limit was neither as obvious nor as important at lower screen voltage (i.e. specific impulse) levels.

The perveance and crossover current limits identified in Fig. 8 correspond, to current conditions at which beamlet ions impact directly on the accelerator grid. At the perveance limit they follow trajectories that are straight and they are drawn from a flatter sheath as the inset sketch suggests. At the crossover current limit, the sheath is more concave and some trajectories cross. In between these two limits, the impingement current is at a low (baseline) level

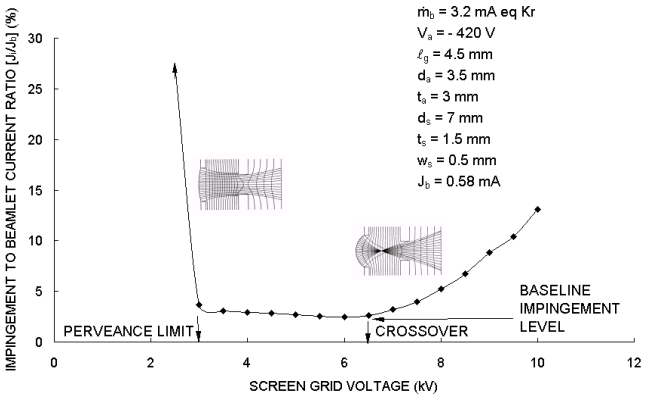

Fig. 8 Effect of Screen Grid Voltage on Accelerator Grid Impingement

where accelerator grid operation in a thruster could be sustained over a long time with low direct ion erosion levels on the accelerator grid. It is noted that the beamlet current (J_b) cited on Fig. 8 is a nineteenth of the beam current actually measured during the test.

For this study, where the net acceleration voltage is fixed by the mission, it is more useful to vary beam current while holding net acceleration voltage constant and to plot impingement-to-beamlet current ratio against beamlet current to identify the perveance and crossover limits. Figure 9 shows data obtained following this procedure for cases where the grid separation (ℓ_g) was varied from 7 to 11.5 mm.

Curves through these data also show that there are indeed beamlet currents at which impingement currents begin to change rather suddenly. However, these curves differ from those in Fig. 8 in the following ways:

- The baseline impingement-to-beam current ratio is substantially greater in Fig. 9 than it is in Fig. 8. This difference is due to the greater Kr flow required to achieve the highest beamlet current (~4 mA). This results in substantially greater charge exchange (CE) ion production, which yields greater impingement currents for the Fig. 9 data.
- The Fig. 9 data exhibit a baseline impingement-to-beamlet current ratio that increases as beamlet current is reduced while the one in Fig. 8 obtained at a constant beamlet current was quite flat. This difference is also related to the greater flow rate and to the fact that the unionized propellant loss rate and, therefore, the impingement current increase as beamlet current is reduced. If flow rate is reduced along with beamlet current, baselines for data like those in Fig. 9 become more nearly horizontal.

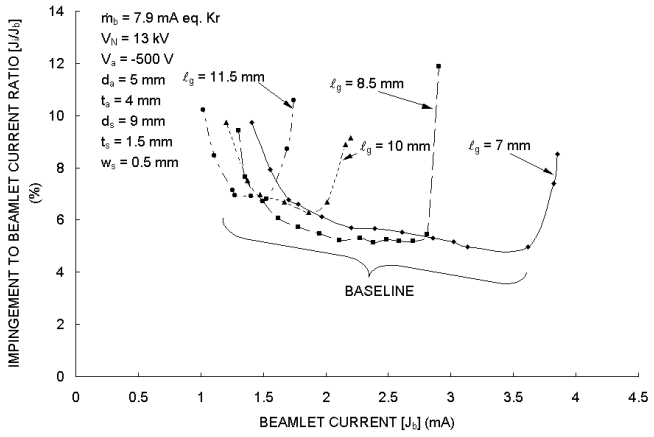

Fig. 9 Typical Effect of Beamlet Current and Grid Spacing on Impingement Current

In order to determine the crossover and perveance limits on beamlet current from experimental data like those from Fig. 9, the approach suggested by Fig. 10

was used. Specifically, it was determined that the data generally fell into three groupings that could each be fit using linear least-squares analysis. The intersections of these three lines defined the limits suggested in the figure.

When the beamlet current limits from plots like those in Fig. 9 associated with direct interception of ion trajectories on the accelerator grid (i.e. the perveance limit) were interpreted as shown in Fig. 10, results identified by the solid symbols and light lines in Fig 11 were obtained. Also identified in this figure by the open symbols and heavier lines are corresponding numerical results obtained using the "igx" code. The agreement between these data is reasonably good for the closer grid separations and larger accelerator holes but agreement is poorer for greater separation. As expected the perveance limited beamlet current increases as accelerator grid hole diameter is increased or grid separation is reduced.

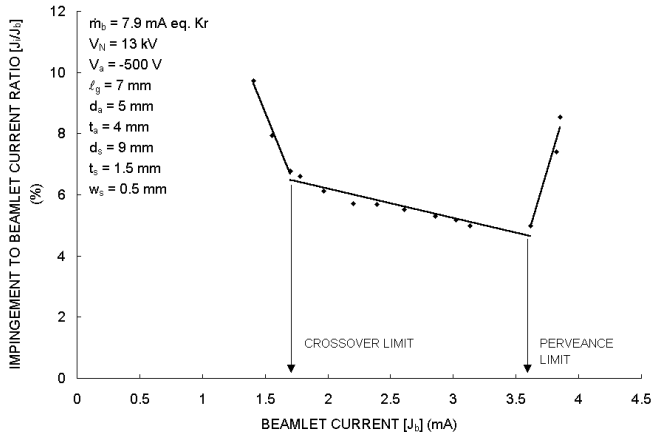

Fig. 10 Determination of Crossover and Perveance Limited Beamlet Currents

When crossover limited beamlet current experimental and numerical data are plotted as a function of the grid parameters being investigated, the results of Fig. 12 are obtained. These two sets of data generally show similar trends, but the experimental data are about 0.5 mA/hole less than the numerical data. This suggests numerically predicted sheath shapes are affected less by beamlet current than are the experimental ones. There is experimental evidence which suggests a flow rate effect may be the source of this difference, possibly because it influences the sheath through the discharge chamber electron temperature.

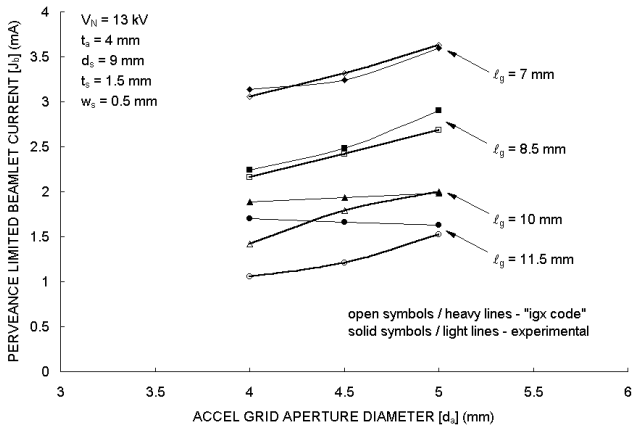

Fig. 11 Effect of Grid Spacing and Accelerator Hole Diameter on Perveance Limit

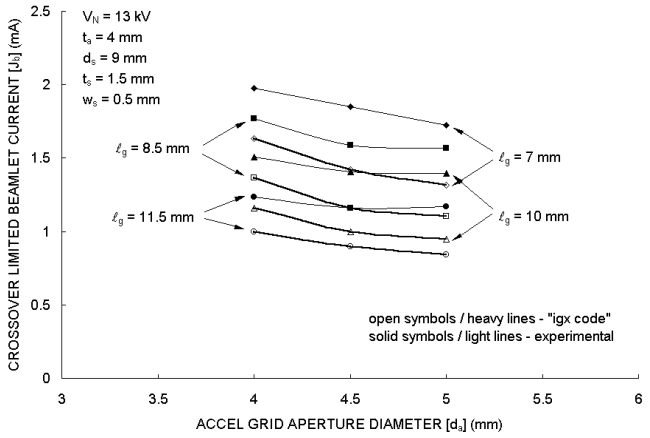

Fig. 12 Effect of Grid Spacing and Accelerator Hole Diameter on Crossover Limit

All of the data in Fig. 12 show that greater grid separation results in a lower crossover limit. This may occur because sheath distortion dimensions become smaller fractions of the effective acceleration length, which appears in the expression for perveance, as the grid separation is increased.

Discussion

Generalization of Results

It is desirable to correlate beamlet current limits like those given in Figs. 11 and 12 using an appropriate physical model. For these data, that model would be based on the Child-Langmuir Law [6] and the limits

would be expressed in terms of a new normalized perveance/hole given by the expression:

$$\wp = \left(\frac{J_b}{V_T^{3/2}} \left[\frac{\ell_e}{d_s} \right]^2 \right) \left(\frac{9}{\pi \varepsilon_o} \sqrt{\frac{m}{2e}} \right). \quad (1)$$

In this expression, the effective acceleration length (ℓ_e) can be approximated using

$$\ell_e = \sqrt{(\ell_g + t_s + \ell_{sh})^2 + d_s^2/4} \quad (2)$$

For the case of the perveance limited beamlet current where the sheath could be expected to be near the upstream side of the screen grid the sheath-screen grid separation (ℓ_{sh}) could be assumed to be zero. Perveances associated with all of the experimental perveance limited beamlet current data from Fig. 11 were calculated under this assumption using Eqs. (1) and (2). Mean values of these results are plotted against normalized accelerator grid aperture diameter as the solid squares and fine line in Fig. 13.

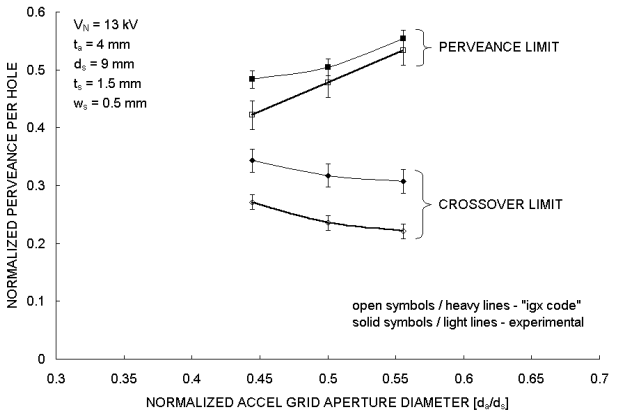

Fig. 13 Correlation of Perveance and Crossover Limit Data

As the error bars through these symbols suggest, the associated standard deviations are not too large and this indicates that the sheath and perveance model assumptions are reasonable.

In order to develop a similar curve for the crossover limited beamlet current data of Fig. 12, it was necessary to model the sheath separation from the screen grid web surface (ℓ_{sh}). This was done by selecting sheath separations for each data point that yielded the best least-squares-regression fit of the Child-Langmuir model. The values of ℓ_{sh} ranged from 0.09 mm at a grid separation of 7 mm to about 0.19 mm at a grid separation of 11.5 mm. The resulting mean and standard deviation results are represented by the solid diamonds and error bars in Fig. 13. Again, their relatively small size suggests the collective data are modeled reasonably well.

Perveance values associated with the perveance and crossover limited beamlet currents were also calculated using the "igx" code. Mean values and standard deviations were again determined for all grid separations studied and the results are represented in Fig. 13 by the open symbols and heavy lines. In doing these calculations, the actual screen-surface-to-sheath separation distances determined by the code were used in Eq. (2). Figure 13 shows similar trends for both the experimental and numerical results. As expected, increases in accelerator grid hole diameter widen the operating margin between the perveance and crossover limits. It is noted that experimental data collected at a net accelerating voltage of 10 kV gave essentially identical results as those for the 13 kV that are shown in Fig.13.

Thruster Design Implications

It is of interest to investigate the impact of the findings of this study on a typical high specific impulse mission. This will be done here by applying typical results from the simple model described in the Appendix of this paper to examine the Interstellar Precursor (ISP) Mission [1]. Input to the analyses will be drawn from "igx" code results because the code yields baseline (i.e. charge-exchange) impingement currents that are more appropriate for a space application than are the experimental results. The code results also yield backstreaming voltage limits of greater magnitude which are, therefore, more conservative.

The beam flatness parameter (F_B) at which a thruster would operate if beamlets were at the perveance limit on the beam centerline and at the crossover limit on the beam edge are calculated using Eq. (A4). This is the minimum flatness parameter at which a thruster having a prescribed grid geometry could be operated with low (baseline) impingement currents across the grids. Of course, the grids could be operated with greater flatness

parameters provided a chamber could be built to produce a sufficiently uniform discharge plasma. The maximum flatness parameter would be unity and grids could be operated at this limit at any beamlet current between the perveance and crossover limits. Figure 14 shows the effect of accelerator grid hole diameter and grid spacing on the minimum flatness parameter at which the grids could be operated as determined from the data of Figs. 11 and 12.

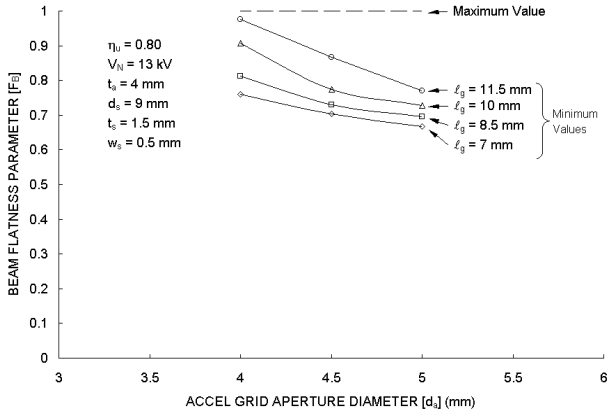

Fig. 14 Limiting Beam Flatness Parameter Limits

Using the flatness parameter results, one can compute the beam diameter required to produce the 2.3-A beam needed for the 30-kW ISP thruster module. Figure 15 shows the effect of grid spacing on this diameter for the three limiting cases (minimum beam flatness and maximum beam flatness at the crossover and perveance beamlet current limits) for a typical accelerator hole diameter (d_a = 4.5 mm). These data show the required diameter ranges from about

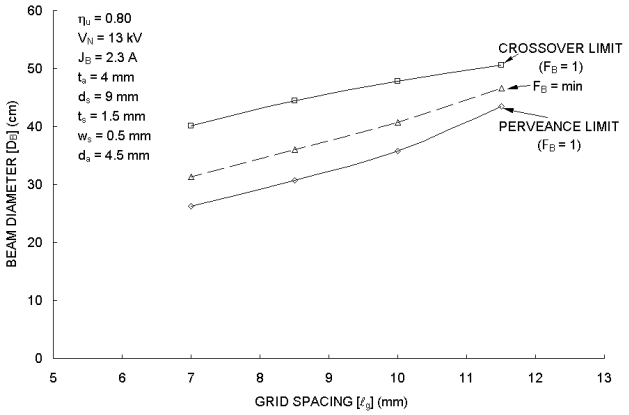

Fig. 15 Beam Diameters Required for 2.3A Beam Current

25 cm for the closest grid spacing with maximum flatness (unity) at the perveance limit to over 50 cm for the greatest grid spacing with maximum flatness at the crossover limit. Discharge chamber operation at the minimum flatness condition yields intermediate diameters as the figure shows. Of course operation at beamlet currents between the crossover and perveance limits also gives intermediate beam diameters. If a greater accelerator hole diameter is used, the range of beam diameters at a given grid spacing is also greater.

Using these results along with similar ones for the other accelerator hole diameters investigated yields the accelerator grid sputter erosion lifetime data shown in Fig. 16. As the legend suggests, they were determined using titanium sputtering data and assuming end-of-life (EOL) when 10% of the accelerator grid mass associated with the most severely eroded hole had been lost to sputter erosion. This number is only approximate and the data of Fig. 16 are, therefore, most useful as indicators of trends. It is noted that a more accurate examination of lifetime would have to consider effects such as those associated redeposition and resputtering which could be important for the thick accelerator grids being considered here.

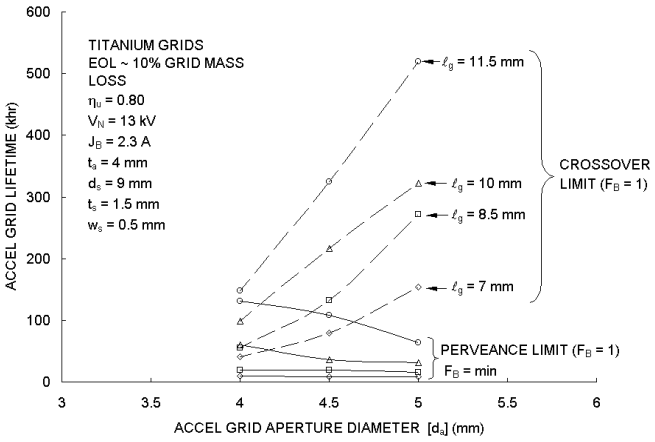

Fig. 16 Accelerator Grid Lifetime Trends

Lives for the cases of minimum beam flatness and unity beam flatness at the perveance limit are represented by the same lines in Fig. 16. These lines fall on top of each other because the life limiting holes are operating at the perveance limit and accelerator grid voltages are not very different for these two cases. These data show greater lifetimes as grid spacing is increased because beam diameter increases and more accelerator grid material is available to be sputtered. They also show

greater lifetimes as accelerator hole diameter is reduced, again because more grid material is available to be sputtered. The greatest lifetimes are realized for operation with unity beam flatness at the crossover limit. Lifetimes become very long at this condition not only because the amount of available grid material is greatest, but also because the backstreaming voltage at which the accelerator grid must be operated is lowest and sputter yields are, therefore, also at their lowest values. Once again it should be noted that operation could occur between any of the corresponding dashed and solid lines (i.e. between the perveance and crossover limits) with the same symbols (e.g. circles).

Conclusions

The range of low accelerator-grid impingement currents in high specific impulse grids is bounded by perveance and crossover limits at high and low beamlet currents, respectively. The crossover limit seems to be more apparent with high specific grids than it was with low specific impulse ones. These limits are strong functions of grid separation and accelerator grid hole diameter.

The accelerator grid voltages that must be applied to stop electron backstreaming in high specific impulse grids are not markedly different than those required at low specific impulse.

If a screen grid is too thin the discharge chamber plasma sheath may be located substantially upstream of the grid surface. Under these conditions a substantial current of ions will be drawn from the region upstream of the screen-grid web, accelerated diagonally across the screen hole axis and onto the upstream side of the accelerator grid

Numerical analysis that appears to be consistent with experimental observations shows that a two-grid ion optics set can be designed that will be reasonable in size and suitable for long duration missions.

Acknowledgement

Financial support under Research Grant NAG3-1801 through the NASA Glenn Research Center is gratefully acknowledged.

References

[1] Patterson, M.J., R.F. Roman, and J.E. Foster, "Ion Engine Development for Interstellar Precursor Missions," AIAA Paper 2000-3811, Joint Propulsion Conference, Huntsville, AL, July 2000.

[2] Wilbur, P.J. and B.W. Buchholtz, "Surface Engineering using Ion Thruster Technology," AIAA Paper 94-3235, p. 2, 30th Joint Propulsion Conference, Indianapolis, IN 1994.

[3] Wilbur, P.J. and L.O. Daniels, "The development and application of an ion implanter based on ion thruster technology," *Vacuum*, v. 36, p 4, 1968.

[4] Nakayama, Y., and P.J. Wilbur, "Numerical Simulation of Ion Beam Optics for Many-grid Systems," AIAA Paper 2001-3782, 37th Joint Propulsion Conference, Salt Lake City, UT, 2001.

[5] Soulas, G.C., J.E. Foster, and M.J. Patterson, "Performance of Titanium Optics on a NASA 30 cm Ion Thruster," AIAA Paper 2000-3814, 36th Joint Propulsion Conference, Huntsville, AL, 2000.

[6] Child, C.D., "Discharge from Hot CaO," *Physics Review*, v. 32, pp. 492-511, 1911.

[7] Wehner, G.K., "Sputter Yield Data in the 100-600 eV Energy Range," General Mills Report 2309, July 15, 1962.

[8] Bohdansky, J., J. Roth and H.L. Bay, "An analytical formula and important parameters for low-energy ion sputtering," *J. Appl. Phys*. **51**, pp. 2681-2865**,** May 1980.

[9] Anderson, J.R., J.E. Polk and J.R. Brophy, "Service Life Assessment for Ion Engines," 25th International Electric Propulsion Conference Paper 97-049, Cleveland, OH 1997.

Appendix
A Model of Thruster Accelerator Grid Erosion

Since much of the appendix nomenclature is not used in the body of this paper, new nomenclature will be

defined as it is used herein. Previously defined nomenclature will also be used.

The ion beam flatness parameter (F_B) for a thruster is defined as the ratio of average beamlet current ($<J_b>$) to peak beamlet current (J_b') i.e.

$$F_B = \langle J_b \rangle / J_b' \; . \qquad \text{(A1)}$$

The average current density can be determined by integrating beamlet currents from the thruster centerline to the beam edge at radius $r_e = D_B/2$ i.e.

$$\langle J_b \rangle = \frac{\int_0^{r_e} J_b \, 2\pi r \, dr}{\pi r_e^2} \; . \qquad \text{(A2)}$$

If it is assumed that the current density profile has a cosine shape then

$$J_b = J_b' \cos\left(\frac{\pi r}{2 r_r}\right) \qquad \text{(A3)}$$

where r_r is a reference radius that is greater than r_e. Substituting Eq. (A3) into Eq. (A2) and integrating gives the result

$$F_B = \frac{2}{\alpha}\left[\frac{1}{\alpha}\{\cos\alpha - 1\} + \sin\alpha\right] \qquad \text{(A4)}$$

where $\alpha = \dfrac{\pi r_e}{2 r_r}$.

For the case of a thruster operating at minimum F_B the centerline beamlet current would be at the perveance limit and the grid-edge beamlet current (i.e. at $r = r_e$) would be at the crossover limit. Using these limits in Eq. (A3) one obtains a value for α which can then be used in Eq. (A4) to obtain the flatness parameter.

The number of screen/accelerator hole pairs with average beamlet current $<J_b>$ that are required for a beam current J_B is

$$n = \frac{J_B}{\langle J_b \rangle} \; . \qquad \text{(A5)}$$

The hexagonal area occupied by a screen hole and its associated webbing can be expressed in terms of the screen hole diameter (d_s) and the minimum webbing thickness (w_s). Dividing this area into the area of the thruster beam ($\pi D_B^2/4$) also yields the number of holes. Combining these results with Eq. (A1) and solving for the beam current one obtains:

$$J_B = \frac{\pi F_B J_b'}{2\sqrt{3}}\left(\frac{D_B}{d_s + w_s}\right)^2 . \qquad \text{(A6)}$$

When beam current is specified (as it is in the present case) this equation can be rearranged and solved for the beam diameter.

The estimate of accelerator grid lifetime used for this study was obtained by assuming end of life was reached when a specified fraction of the initial mass associated with the most severely eroded hole had been lost. The initial mass of the hexagonal region of area A_b associated with each accelerator hole beamlet is given by

$$m_a = A_b \, t_a \, (1 - \phi_a) \, \rho_a \qquad \text{(A7)}$$

where t_a, ϕ_a and ρ_a are the thickness, transparency and mass density of the accelerator grid, respectively. The mass loss per accelerator grid beamlet induced by sputtering over a time τ is given by

$$\Delta m_a = \frac{J_i \, Y \, M \, \tau}{e} \qquad \text{(A8)}$$

where J_i is the impingement current per beamlet, Y is the sputter yield for Kr ions on the accelerator grid material, M is the mass of a grid material atom and e is the electron charge.

If it is assumed that grid failure occurs when the accelerator grid mass-loss fraction associated with the beamlet operating at the greatest impingement current reaches a prescribed value (f_f) one has

$$\Delta m_a = f_f \, m_a . \qquad \text{(A9)}$$

The equation for the yield that is required in Eq. (A8) was obtained by fitting experimental data [7] to an empirical expression [8]. The result obtained for krypton ions impacting titanium is

$$Y = 0.47 \left(\frac{E}{68} \right)^{1/4} \left(1 - \frac{68}{E} \right)^{3.5} . \quad \text{(A10)}$$

If it is assumed that most of the impinging ions are produced near the accelerator grid, the energy (E) that is needed in this equation can be estimated. It has been suggested that it has a magnitude equal to the accelerator grid voltage relative to spacecraft ground plus the voltage difference between spacecraft ground and the mean beam plasma potential at which charge-exchange ions are produced. This voltage difference has been estimated to be ~20 V for the NSTAR thruster [9]. Using this value

$$E = \left| V_a \right| + 20 . \qquad \text{(A11)}$$

Combining Eqs. (A7), (A8) and (A9) and solving for grid lifetime one obtains

$$\tau = \frac{\pi f_f \, t_a \, \rho_a \, e}{4 \, Y \, M \, J_i} \left(\frac{2\sqrt{3}}{\pi} (d_s + w_s)^2 - d_a^2 \right) \qquad \text{(A12)}$$

where J_i is the maximum impingement current per beamlet encountered over the entire accelerator grid. For the results presented in this paper, the impingement currents are associated only with thruster generated charge-exchange ions. Because charge exchange ion production associated with test facility effects are not included, the currents are considered to be representative of the space environment. These currents were determined using the "igx" computer code.